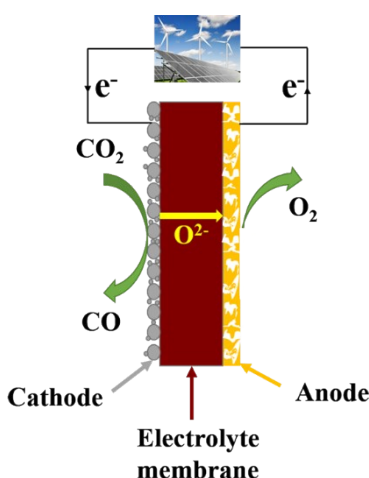


## Supplementary Information

### Iron stabilized 1/3 A-site deficient La-Ti-O perovskite cathodes for efficient CO<sub>2</sub> electroreduction

Shiqing Hu, Lixiao Zhang, Lili Cai, Zhongwei Cao, Qike Jiang, Wenguang Yu, Yongkuan Wu, Xuefeng Zhu,\* and Weishen Yang\*



Scheme S1. Working principles of SOECs.

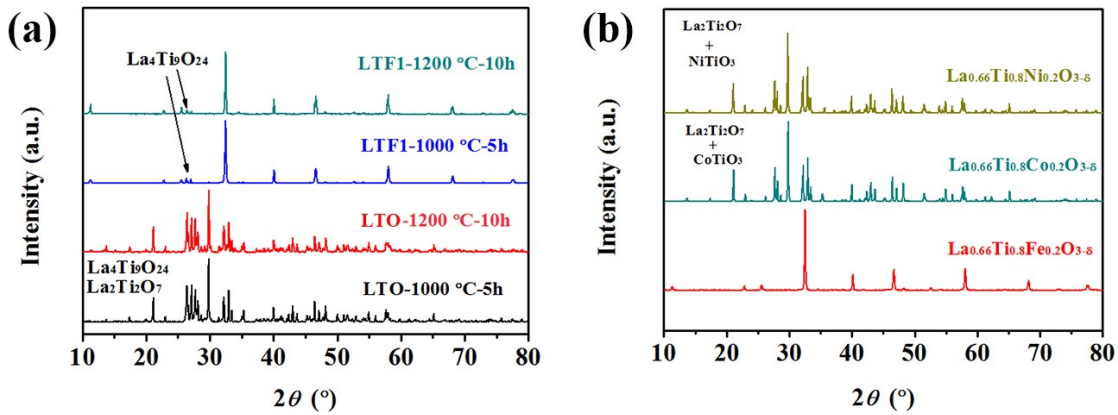


**Figure S1.** Phase structure characterizations: (a) XRD results of  $\text{La}_{0.66}\text{TiO}_3$  (LTO) and  $\text{La}_{0.66}\text{Ti}_{0.9}\text{Fe}_{0.1}\text{O}_{3-\delta}$  (LTF1) calcined at different conditions; (b) XRD results of  $\text{La}_{0.66}\text{Ti}_{0.8}\text{Ni}_{0.2}\text{O}_{3-\delta}$  (LTN2),  $\text{La}_{0.66}\text{Ti}_{0.8}\text{Co}_{0.2}\text{O}_{3-\delta}$  (LTCo2) and LTF2 calcined at 1000 °C for 5 h in Air.

Under the same synthesis conditions,  $\text{La}_{0.66}\text{TiO}_3$  does not show perovskite structure but a mixture of  $\text{La}_2\text{Ti}_2\text{O}_7$  and  $\text{La}_4\text{Ti}_9\text{O}_{24}$  (**Figure S1 a**). It seems that Fe cations are vital during perovskite structure formation process, because LTN2 and LTCo2 do not demonstrate typical perovskite diffraction peaks either (**Figure S1 b**). There is a lower solubility limit (>10% in B-site) of Fe cations in these Ti-based perovskite oxides. Pure perovskite structure will not form if Fe content is too low.

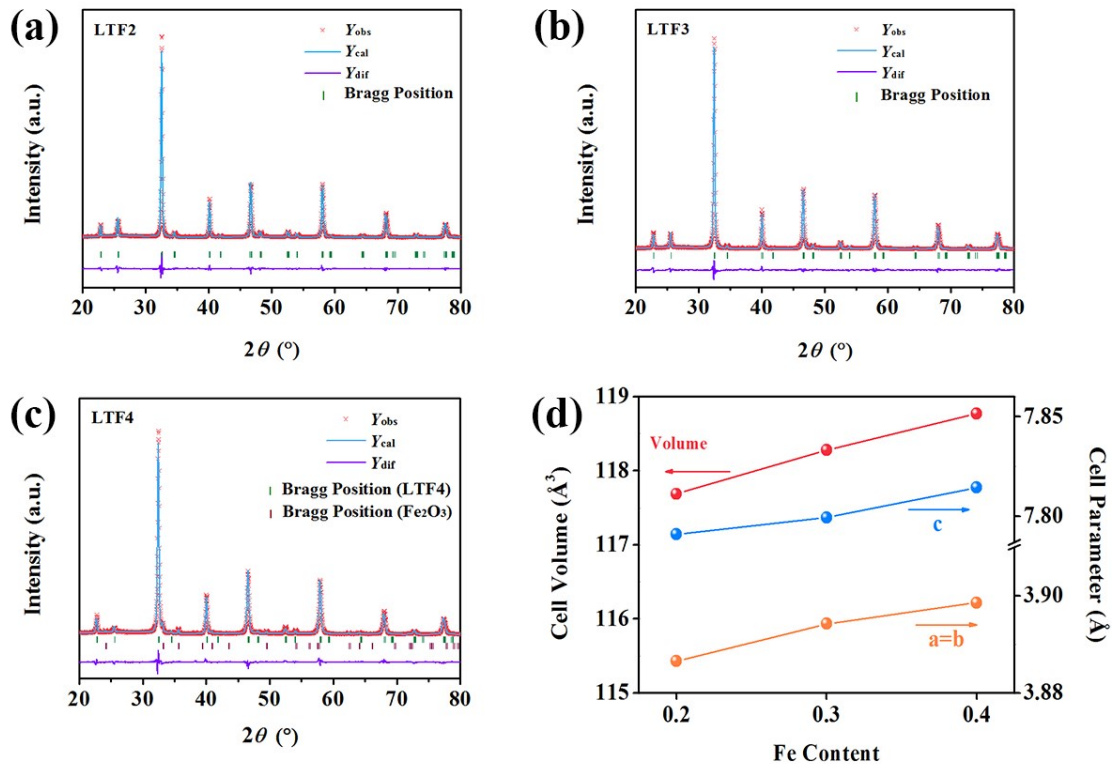


**Figure S2.** Rietveld refinement results of (a) LTF2, (b) LTF3 and (c) LTF4; (d) the relationship between cell parameters and Fe content.

**Table S1.** Rietveld refinements results of LTF2, LTF3 and LTF4.

Sample	Space group	a (Å)	b (Å)	c (Å)	$R_{wp}$ (%)	$R_p$ (%)	$\chi^2$
LTF2	P4/mmm	3.8866	3.8866	7.7910	11.66	8.49	2.94
LTF3	P4/mmm	3.8942	3.8942	7.7994	10.97	7.46	2.65
LTF4	P4/mmm	3.8986	3.8986	7.8144	9.99	7.6	2.19

**Table S2.** The hyperfine parameters of  $^{57}\text{Fe}$  Mössbauer spectra for LTF2, LTF3 and LTF4.

Sample	Fe species	IS (mm s <sup>-1</sup> )	QS (mm s <sup>-1</sup> )	$\Gamma$ (mm s <sup>-1</sup> )	$B_{hf}$ (T)	$\chi^2$
LTF2	doublet	0.36	0.59	0.38	-	1.11
LTF3	doublet	0.37	0.59	0.38	-	1.47
LTF4	doublet	0.36	0.57	0.37	-	1.11
	sextet	0.37	-0.22	0.25	51.59	

IS, QS,  $\Gamma$ ,  $B_{hf}$  and  $\chi^2$ , respectively, represent isomer shift, quadrupole splitting, line width, magnetic hyperfine field and goodness of fitting. IS originates from the electric monopole interaction and related to the oxidation of Fe. QS is caused by the electric dipole interaction and provides the information of  $\text{Fe}^{3+}$  site disorder<sup>[1]</sup>. The magnetic hyperfine interaction will split  $\text{Fe}^{3+}$  Mössbauer spectra into sextets due to the intrinsic or externally applied magnetics hyperfine fields. As shown in **Table S2**, all the Fe species shows similar IS of 0.36-0.37 mm s<sup>-1</sup>. These values of IS conform to  $\text{Fe}^{3+}$ . These non-zero QS (0.57-0.59 mm s<sup>-1</sup>) means  $\text{Fe}^{3+}$  sites deviate from the cubic symmetry. As shown in **Figure 1 d**, these perovskite oxides show tetragonal structure with P4/mmm space group. The only one doublet used to fit the Mössbauer spectra implies  $\text{Fe}^{3+}$  in the perovskite lattice is paramagnetic and has the same occupation site. The sextet with  $B_{hf}$  of 51.59 T in LTF4 is attributed to  $\text{Fe}^{3+}$  in  $\text{Fe}_2\text{O}_3$ . All the  $\chi^2$  is close to 1, verifying the reliability of the fitting models.

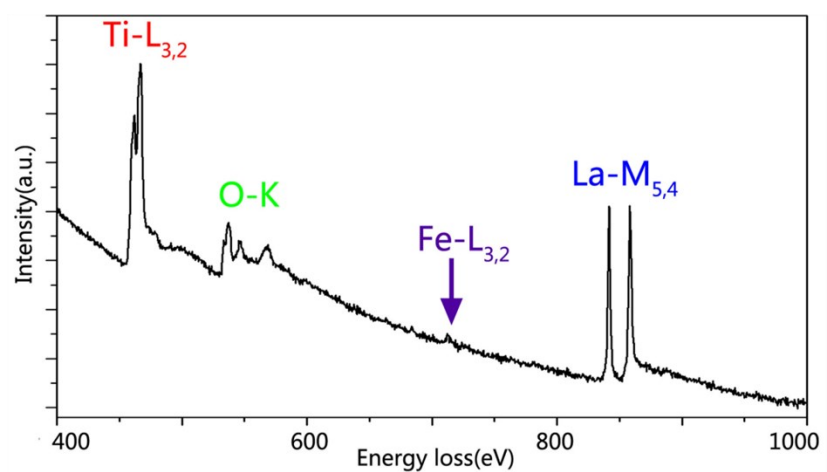


**Figure S3.** EELS signals for elements (La, Ti, Fe and O) in LTF2. EELS signals show the existence of La, Ti, Fe and O.

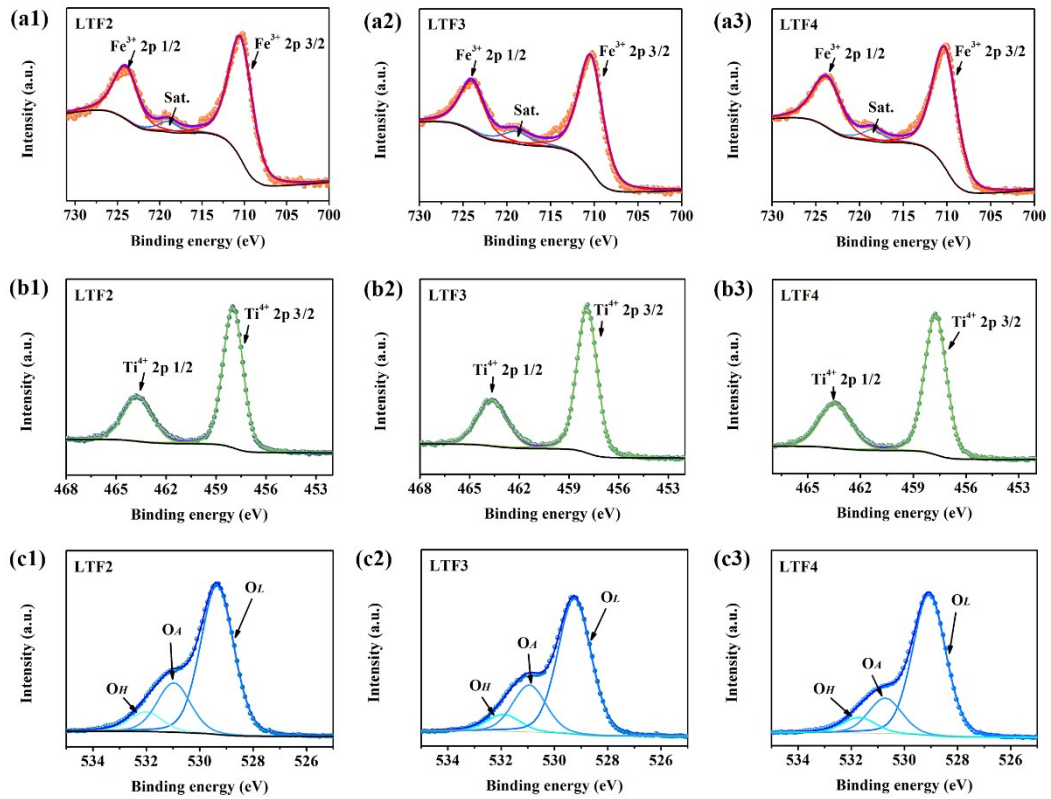


**Figure S4.** XPS analysis of LTF2, LTF3 and LTF4. (a1)-(a3) Fe 2p; (b1)-(b3) Ti 2p and (c1)-(c3) O1s.

**Table S3** O1s fitting results of LTF2, LTF3 and LTF4.

Sample	Binding energy (eV)			Relative concentration (%)		
	O <sub>L</sub>	O <sub>A</sub>	O <sub>H</sub>	O <sub>L</sub>	O <sub>A</sub>	O <sub>H</sub>
LTF2	529.35	530.97	532.02	68.37	22.66	8.97
LTF3	529.25	530.94	531.91	68.00	23.56	8.44
LTF4	529.07	530.72	531.69	73.49	18.42	8.09

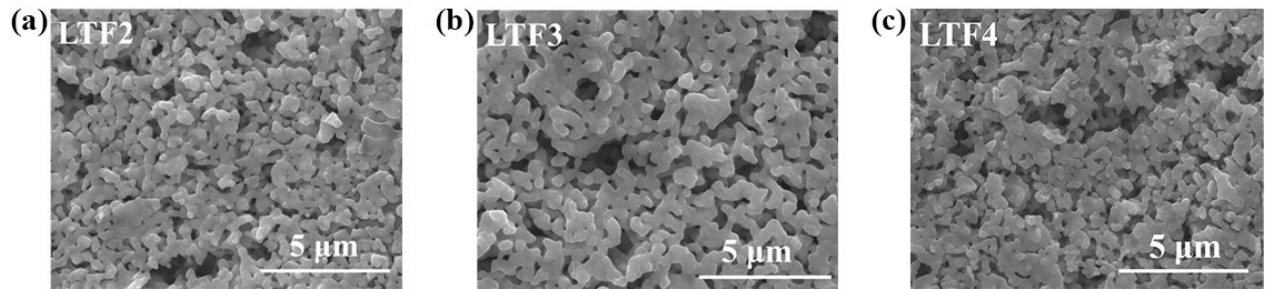


**Figure S5.** SEM images of (a) LTF2, (b) LTF3 and (c) LTF4 cathode after sintering at 1100 °C for 2 h.

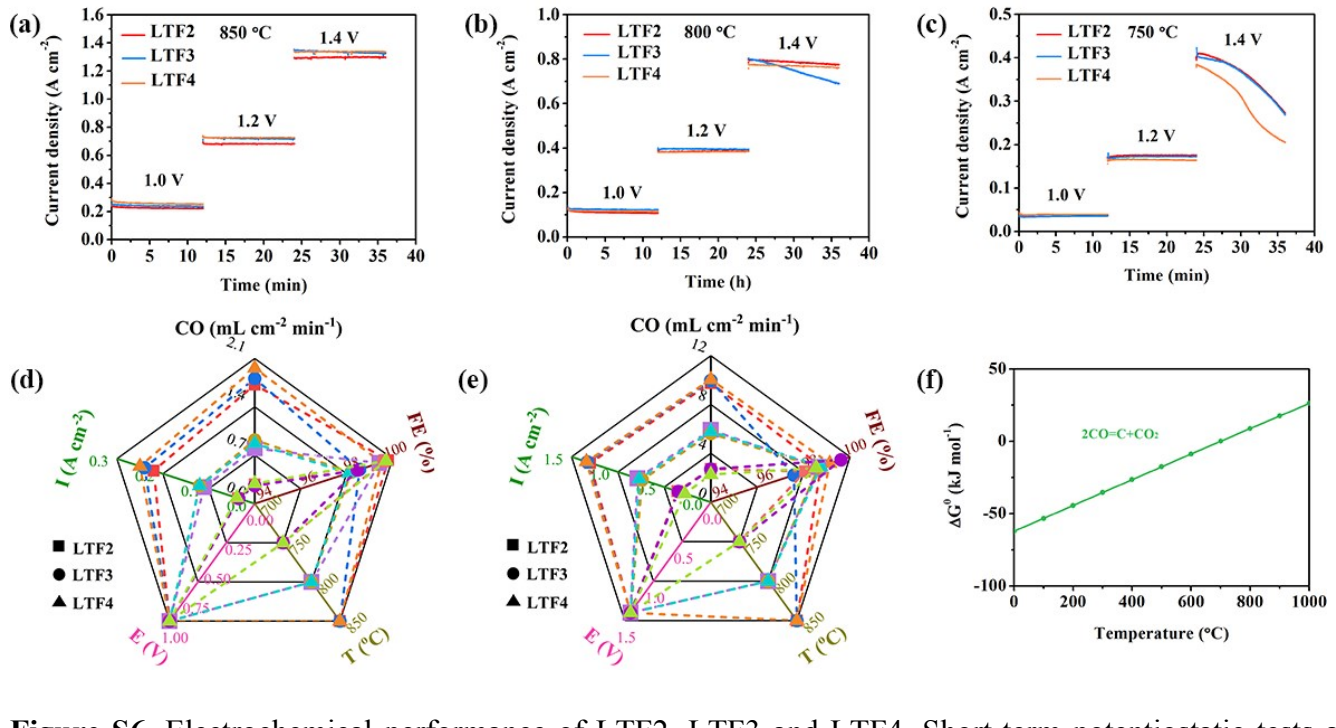


**Figure S6.** Electrochemical performance of LTF2, LTF3 and LTF4. Short-term potentiostatic tests at (a) 850 °C, (b) 800 °C and (c) 750 °C; electrochemical performances at (d) 1.0 V and (e) 1.4 V from 750 °C to 850 °C, including current density (I), CO production rate (CO) and Faradic efficiency (FE); (f) standard Gibbs free energy of Boundouard reaction at different temperatures.

**Table S4.** The current density, CO production rate and Faradic efficiency of LTF2, LTF3 and LTF4 at different conditions.

Cathode	Temperature	750 °C			800 °C			850 °C		
		1.0	1.2	1.4	1.0	1.2	1.4	1.0	1.2	1.4
LTF2	Current density (A cm <sup>-2</sup> )	0.037	0.18	0.36	0.11	0.39	0.79	0.22	0.68	1.30
	CO production rate (mL cm <sup>-2</sup> min <sup>-1</sup> )	0.28	1.32	2.72	0.80	2.93	5.92	1.72	5.17	9.76
	Faradic efficiency (%)	99.9	99.2	98.2	99.7	99.9	98.8	100.1	99.5	98.9
LTF3	Current density (A cm <sup>-2</sup> )	0.035	0.17	0.35	0.12	0.40	0.74	0.24	0.72	1.33
	CO production rate (mL cm <sup>-2</sup> min <sup>-1</sup> )	0.26	1.31	2.70	0.92	2.98	5.63	1.81	5.40	9.96
	Faradic efficiency (%)	98.7	100	99.8	98.4	98.8	98.8	98.8	98.8	97.7
LTF4	Current density (A cm <sup>-2</sup> )	0.039	0.16	0.28	0.12	0.38	0.77	0.25	0.73	1.34
	CO production rate (mL cm <sup>-2</sup> min <sup>-1</sup> )	0.29	1.25	2.26	0.87	2.88	5.79	1.96	5.49	10.04
	Faradic efficiency (%)	100.0	99.6	98.7	98.3	99.3	98.9	99.8	99.7	99.3

As shown in **Figure 2 b**, **Figure S6** and **Table S4**, these cathodes of LTF2, LTF3 and LTF4 show similar electrochemical performances towards CO<sub>2</sub> electroreduction. It is noted that the stability at 1.4 V becomes worse as the temperature decreases. During test process, the performance recovery at 1.4 V and 750 °C was observed after CO<sub>2</sub> swept the cathode for few minutes without applied voltage. It is speculated that carbon deposition occurs at 1.4 V and 750 °C. It is widely accepted that carbon deposition occurs through Boudouard reaction (2CO=C+CO<sub>2</sub>)<sup>[2]</sup>. **Figure S6 f** shows the standard Gibbs free energy of Boudouard reaction at different temperature. The Gibbs free energy decreases as the temperature decreases, implying lowering temperature promotes carbon deposition. When the applied voltage is cut off, deposited carbon will be removed through the reversed Boudouard reaction (CO<sub>2</sub>+C=2CO). Then the performance recovers as before.

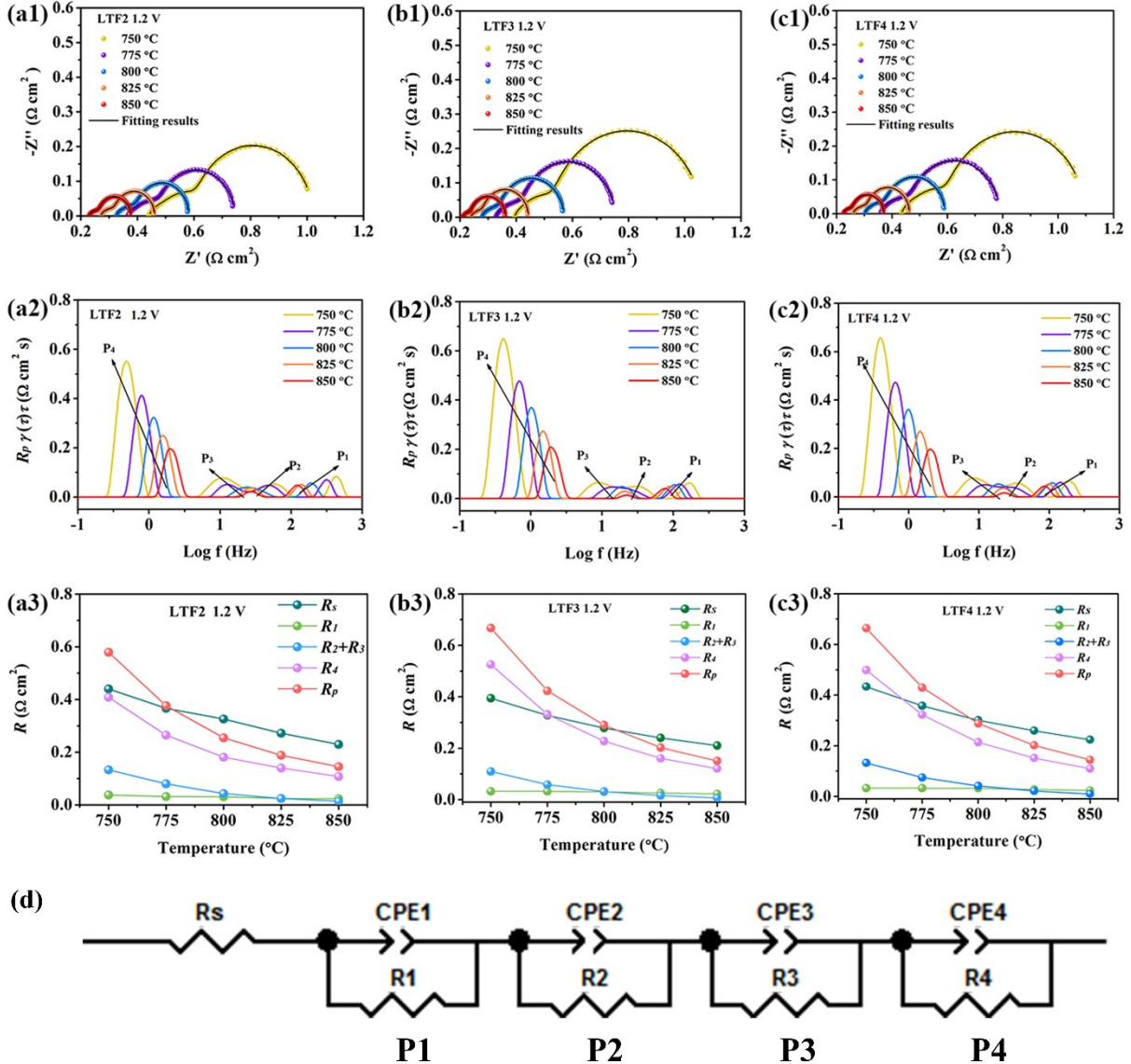


**Figure S7.** Kinetics process analysis at 1.2 V and different temperatures. (a1)-(c1) EIS of LTF2, LTF3 and LTF4; (a2)-(c2) DRT analysis; (a3)-(c3) the result of fitting resistances and (d) equivalent circuit model used for EIS fitting.

**Table S5.** The fitting resistances of LTF2, LTF3 and LTF4 at 1.2 V and different temperatures.

Cathode	Resistance ( $\Omega \text{ cm}^2$ )	$R_s$	$R_I$	$R_2$	$R_3$	$R_4$	$R_p$
<b>LTF2</b>	750 °C	0.440	0.0377	0.0481	0.085	0.409	0.580
	775 °C	0.367	0.032	0.039	0.041	0.265	0.377
	800 °C	0.326	0.031	0.043		0.181	0.255
	825 °C	0.272	0.024	0.020		0.140	0.184
	850 °C	0.229	0.023	0.014		0.108	0.145
<b>LTF3</b>	750 °C	0.394	0.032	0.041	0.068	0.525	0.666
	775 °C	0.328	0.033	0.059		0.332	0.424
	800 °C	0.279	0.031	0.032		0.228	0.291
	825 °C	0.240	0.026	0.016		0.161	0.203
	850 °C	0.210	0.023	0.007		0.121	0.151
<b>LTF4</b>	750 °C	0.434	0.033	0.051	0.082	0.499	0.665
	775 °C	0.358	0.033	0.029	0.045	0.323	0.430
	800 °C	0.302	0.032	0.042		0.214	0.288
	825 °C	0.260	0.028	0.022		0.152	0.202
	850 °C	0.224	0.024	0.010		0.110	0.144

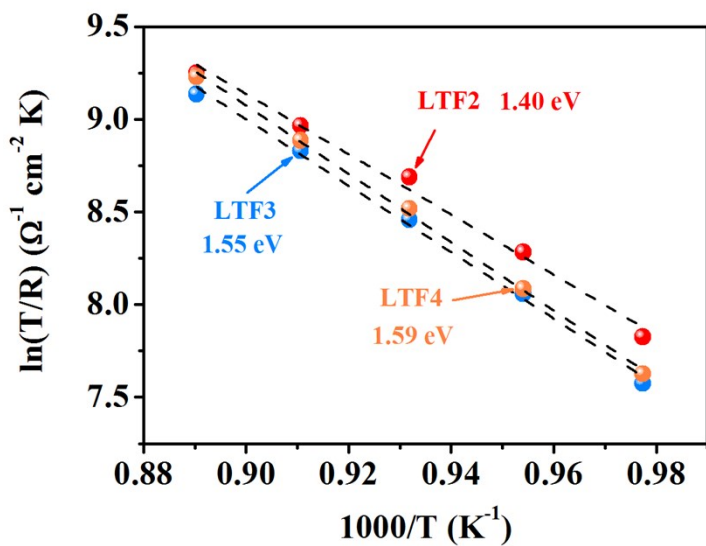


**Figure S8.** Activation energy of LTF2, LTF3, LTF4 for CO<sub>2</sub> conversion at 1.2 V.

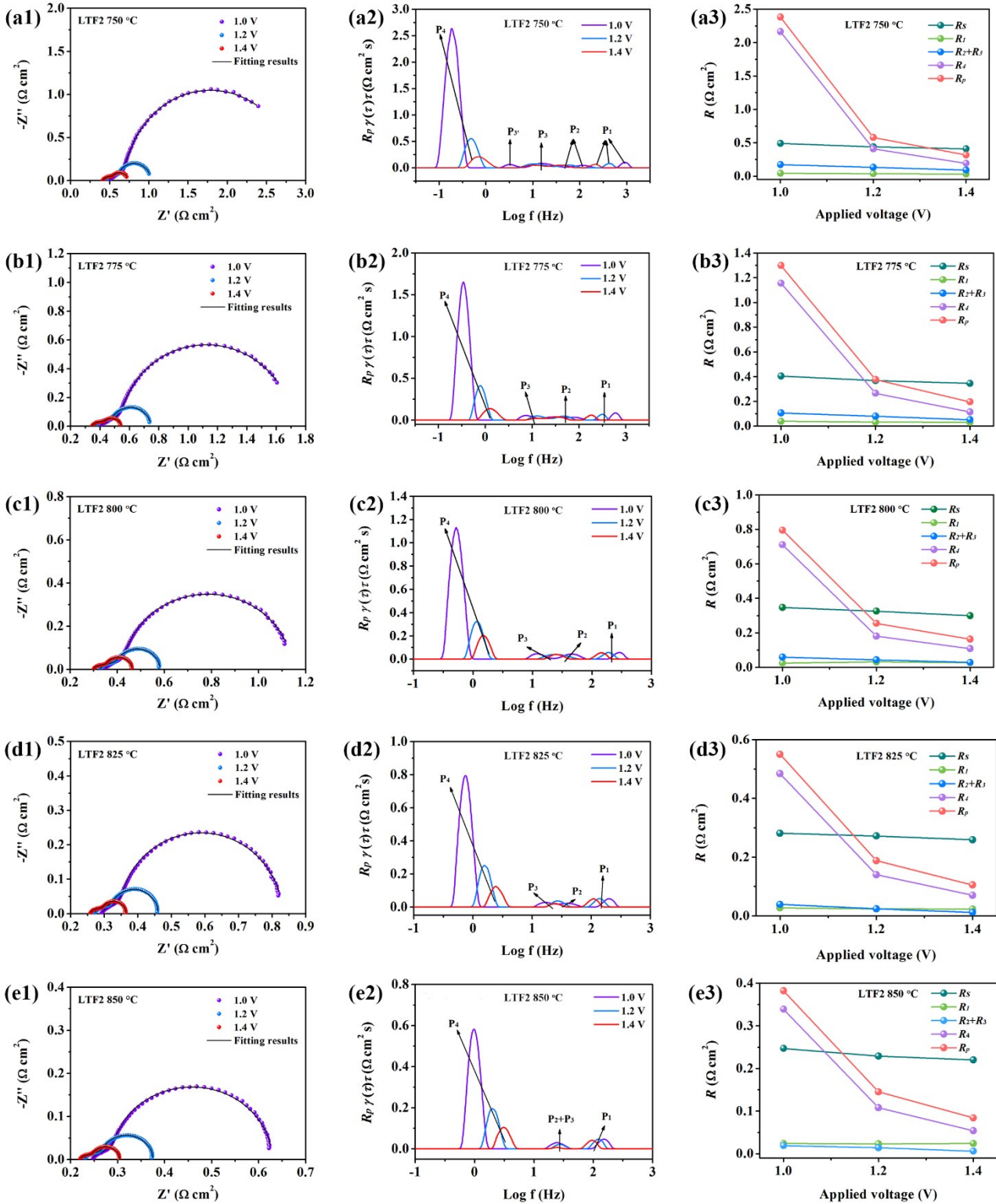


**Figure S9.** Kinetics process analysis of LTF2 at different temperatures and voltages. (a1)-(e1) EIS; (a2)-(e2) DRT analysis; (a3)-(e3) fitting results of resistances.

**Table S6.** The fitting resistances of LTF2 at different temperatures and voltages.

LTF2										
Voltage	Resistance ( $\Omega \text{ cm}^2$ )	$R_s$	$R_I$	$R_2$	$R_3$		$R_4$	$R_p$		
1.0 V	750 °C	0.490	0.044	0.038	0.097	0.038 ( $R_3'$ )	2.164	2.381		
	775 °C	0.405	0.038	0.025	0.039	0.042 ( $R_3'$ )	1.155	1.299		
	800 °C	0.347	0.025	0.031	0.028		0.711	0.795		
	825 °C	0.281	0.027	0.017	0.022		0.484	0.550		
	850 °C	0.247	0.024	0.019			0.339	0.382		
1.2 V	750 °C	0.440	0.038	0.048	0.085		0.409	0.580		
	775 °C	0.367	0.032	0.039	0.041		0.265	0.377		
	800 °C	0.326	0.031	0.043			0.181	0.255		
	825 °C	0.272	0.024	0.024			0.14	0.188		
	850 °C	0.229	0.023	0.014			0.108	0.145		
1.4 V	750 °C	0.410	0.032	0.046	0.046		0.193	0.317		
	775 °C	0.345	0.030	0.038	0.014		0.114	0.196		
	800 °C	0.299	0.027	0.028			0.108	0.163		
	825 °C	0.259	0.023	0.012			0.070	0.105		
	850 °C	0.22	0.024	0.006			0.054	0.084		

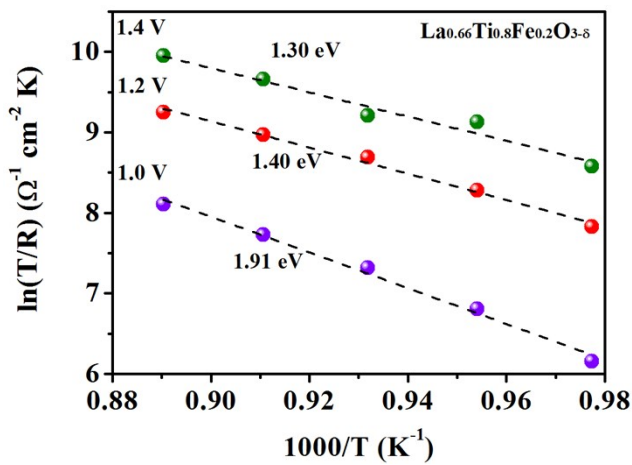


**Figure S10.** The activation energy of LTF2 towards the process of  $\text{CO}_2$  conversion at different voltages.

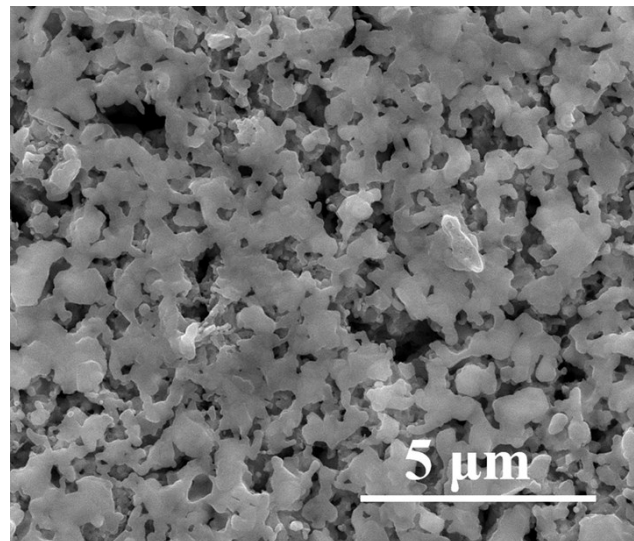


**Figure S11.** SEM image of LTF2 after 300 h potentiostatic test at 1.2 V and 850 °C.

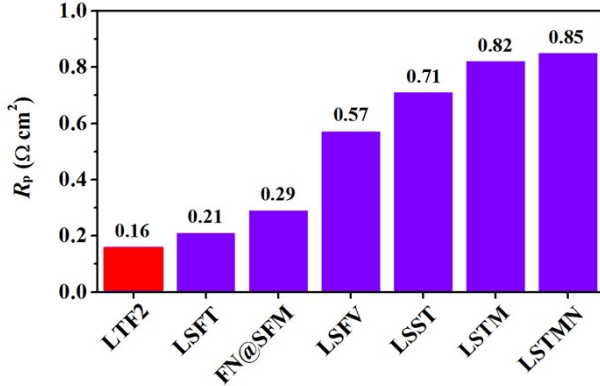


**Figure S12.** Polarization resistance ( $R_p$ ) comparisons with other reported perovskite cathodes at 800 °C and similar applied voltages: LTF2:  $\text{La}_{0.66}\text{Ti}_{0.8}\text{Fe}_{0.2}\text{O}_{3-\delta}$  (1.4 V, this work), LSFT:  $\text{La}_{0.3}\text{Sr}_{0.7}\text{Fe}_{0.7}\text{Ti}_{0.3}\text{O}_3$  (1.4 V)<sup>[3]</sup>, FN@SFM:  $\text{FeNi}_3@\text{Sr}_2\text{Fe}_{1.5}\text{Mo}_{0.5}\text{O}_{6-\delta}\text{-Sm}_{0.2}\text{Ce}_{0.8}\text{O}_{2-\delta}$ <sup>[4]</sup>, LSFV:  $\text{La}_{0.5}\text{Sr}_{0.5}\text{Fe}_{0.95}\text{V}_{0.05}\text{O}_{3-\delta}$  (1.4 V)<sup>[5]</sup>, LSST:  $(\text{La}_{0.2}\text{Sr}_{0.8})\text{Sr}_{0.1}\text{TiO}_{3+\delta}$  (1.5 V)<sup>[6]</sup>, LSTM:  $\text{La}_{0.18}\text{Sr}_{0.72}\text{Ti}_{0.9}\text{Mn}_{0.1}\text{O}_{3-\delta}$  (1.4 V)<sup>[7]</sup>, LSTMN:  $\text{La}_{0.2}\text{Sr}_{0.8}\text{Ti}_{0.85}\text{Mn}_{0.1}\text{Ni}_{0.05}\text{O}_{3+\delta}$  (1.4 V)<sup>[8]</sup>.

**Table S7.** The performance comparison of LTF2 with other perovskite cathodes at 800 °C.

Cathode	Voltage (V)	Current density ( $\text{A cm}^{-2}$ )	$R_p$ ( $\Omega \text{ cm}^2$ )	Reference
LTF2	1.4	0.79	0.16	This work
LSFT	1.4	0.22	0.21	[3]
FN@SFM	1.4	0.62	0.29	[4]
LSFV	1.4	0.45	0.57	[5]
LSST	1.5	0.40	0.71	[6]
LSTM	1.4	0.25	0.82	[7]
LSTMN	1.4	0.29	0.85	[8]

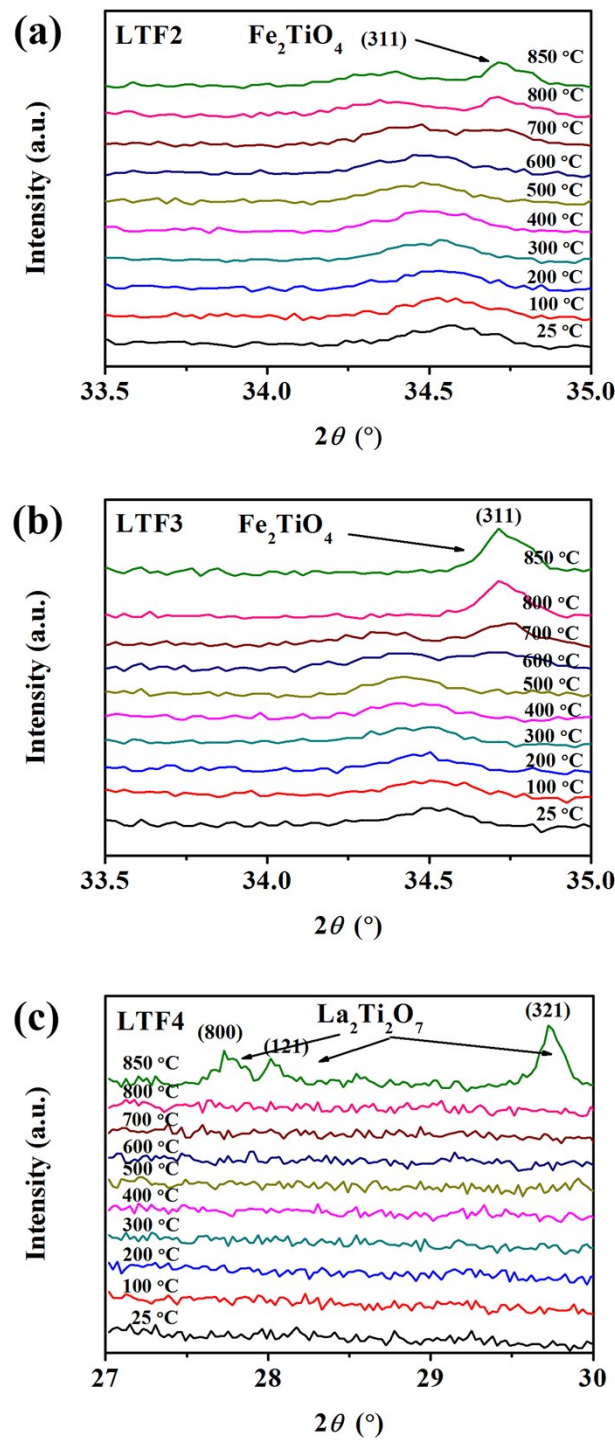


**Figure S13.** The enlarged XRD patterns of (a) LTF2, (b) LTF3 and (c) LTF4 under the simulated electroreduction atmosphere (80% CO - 20% CO<sub>2</sub>) from 25 °C to 850 °C.

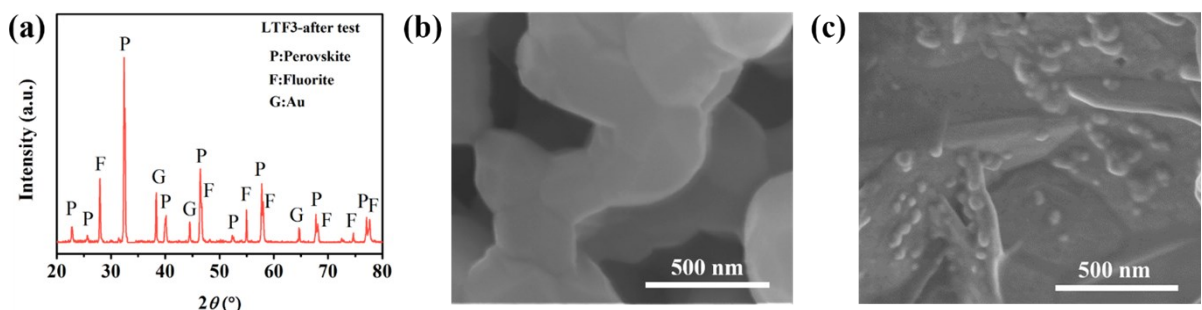


**Figure S14.** Cathode phase structure and surface microstructure evolution after tests: (a) XRD results of LTF3 after electrochemical tests; (b) microstructure of LTF3 before electrochemical tests and (c) microstructure of LTF3 after electrochemical tests.

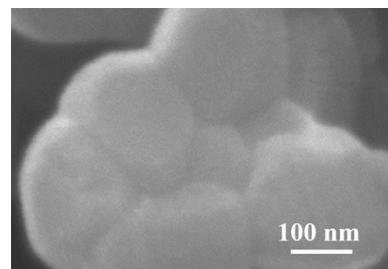


**Figure S15.** SEM image of LTF2 surface before reduction.

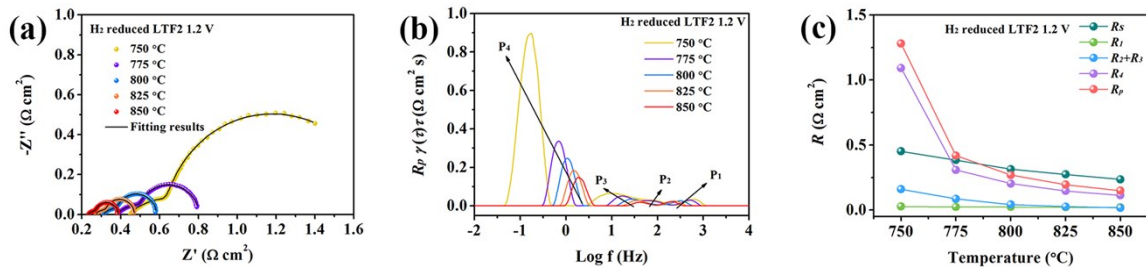


**Figure S16.** Electrode kinetics analysis of R-LTF2 at 1.2 V and different temperature: (a) EIS; (b) DRT analysis combined with EIS; and (d) the fitting results of resistance.

**Table S8.** The fitting results of resistances for R-LTF2 at 1.2 V and different temperatures.

Cathode	Resistance ( $\Omega \text{ cm}^2$ )	$R_s$	$R_l$	$R_2$	$R_3$	$R_4$	$R_p$
RLTF2	750 °C	0.451	0.028	0.039	0.121	1.092	1.280
	775 °C	0.385	0.024	0.025	0.061	0.308	0.418
	800 °C	0.314	0.024	0.042		0.204	0.270
	825 °C	0.274	0.022	0.026		0.147	0.195
	850 °C	0.236	0.019	0.017		0.113	0.149

## References

- [1] a) R. Zboril, M. Mashlan, D. Petridis, *Chem. Mater.* **2002**, *14*, 969; b) K. Zhu, T. Wu, Y. Zhu, X. Li, M. Li, R. Lu, J. Wang, X. Zhu, W. Yang, *ACS Energy Lett.* **2017**, *2*, 1654; c) K. Zhu, C. Jin, C. Zhao, R. Hu, Z. Klencsár, G. Ayyakannu Sundaram, D. F. Sránkó, R. Ge, J. Wang, *Chem. Eng. J.* **2019**, *359*, 1537.
- [2] J. Yan, H. Chen, E. Dogdibegovic, J. W. Stevenson, M. Cheng, X.-D. Zhou, *J. Power Sources* **2014**, *252*, 79.

- [3] Z. Cao, B. Wei, J. Miao, Z. Wang, Z. Lv, W. Li, Y. Zhang, X. Huang, X. Zhu, Q. Feng, Y. Sui, *Electrochim. Commun.* **2016**, *69*, 80.
- [4] H. Lv, L. Lin, X. Zhang, D. Gao, Y. Song, Y. Zhou, Q. Liu, G. Wang, X. Bao, *J. Mater. Chem. A* **2019**, *7*, 11967.
- [5] Y. Zhou, Z. Zhou, Y. Song, X. Zhang, F. Guan, H. Lv, Q. Liu, S. Miao, G. Wang, X. Bao, *Nano Energy* **2018**, *50*, 43.
- [6] L. Ye, C. Pan, M. Zhang, C. Li, F. Chen, L. Gan, K. Xie, *ACS Appl. Mater. Interfaces* **2017**, *9*, 25350.
- [7] L. Ye, X. Hu, X. Wang, F. Chen, D. Tang, D. Dong, K. Xie, *J. Mater. Chem. A* **2019**, *7*, 2764.
- [8] L. Ye, M. Zhang, P. Huang, G. Guo, M. Hong, C. Li, J. T. S. Irvine, K. Xie, *Nat. Commun.* **2017**, *8*, 14785.